Catalogue of P32 observations obtained with the C200 detector

Attila Moór, Péter Ábrahám, Csaba Kiss

2007

Contents

1 Introduction

The P32 Astronomical Observation Template (AOT) of the ISOPHOT instrument was designed to map extended areas of sky with sampling close to the Nyquist limit, using the far-infrared detector arrays (C100, C200) of ISOPHOT (Tuffs & Gabriel, 2003). In order to maximise the spatial resolution this mode combined the coarse raster capability of ISO with the chopping capability of the ISOPHOT instrument in obtaining images. This means that the satellite effective pointing was rapidly modulated in steps of a third of the detector pixel separation using the focal plane chopper. The modulation timescale could be as low as $\sim$0.15 sec. Although this mode provided a good way to observe extended structures with the best achievable spatial resolution, its calibration turned out to be very difficult due to the transient behaviour of the C100 and C200 detectors. The ISOPHOT C200 and especially the C100 detector has a complex non-linear response as a function of illumination history on timescales of $\sim$0.1-100sec, depending on the absolute flux level as well as the flux changes involved (Acosta et al., 2000; Tuffs & Gabriel, 2003). Because of the high frequency flux modulation, a typical P32 observations is in principle always in a non-stabilized state. Due to this fact this mode was not fully exploited scientifically, though later the P32Tools, developed at Max-Planck-Institut für Kernphysik by Richard Tuffs, provided corrections for the transient effects (Tuffs & Gabriel, 2003).

The goal of this catalogue was to extract photometric information from P32 observations obtained with the C200 detector. Our work concentrated on smaller maps (for definition see Sect.2), which were originally designed to measure the flux density of a compact or a slightly extended source.

2 Sample selection

We made a systematic search in the ISO Data Archive (IDA) for ISOPHOT P32 observations obtained with the C200 detector, and selected those maps:

- where raster step numbers were $2 \leq \mathrm{M} \leq 5$ and $1 \leq \mathrm{N} \leq 6$;
- which are not included in the HPDP "Far-Infrared ISOPHOT Photometry of Virgo Cluster Galaxies" (Tuffs et al., 2006);

After data reduction (for details see Sect.3) we selected only those observations, where (1) one or more compact or slightly extended ($<2'$) sources are detected on the final maps; or (2) a known source (e.g. IRAS source, quasar, etc.) is located somewhere in the observed region. In the latter cases the quoted flux density values and their uncertainties can be used to estimate upper limits for the specific objects at wavelengths longer than 100μm.

The final catalogue contains photometry data for 292 measurements in 226 TDTs.

3 Data reduction

Our data processing scheme can be separated into two main levels. At the first processing level we used the **P**HOT **I**nteractive **A**nalysis (PIA) version 10.0 (Gabriel et al., 1997) software combined with separated IDL codes to reduce observations from the lowest data level (Edited Raw Data, ERD) to the final AAP (Auto Analysis Product Data) level. Correction for instrumental effects (e.g. the glitches induced by cosmic particles) as well as flux calibration was performed in this processing phase (see Sect. 3.1 for more details). At the second level, the flux of the target was extracted from the AAP data stream.

3.1 Processing from raw data to AAP level

In the case of many P32 observations – due to the relatively short durations of individual chopper steps – the transient behaviour of the Ge:Ga detectors (C100, C200) leads to systematic errors in the photometry of discrete sources. This effect turned out to be more severe in the case of the C100 detector. The P32Tools, which is now available as integrated part of the PIA v10.0 software package, provides a means of corrections for the complex non-linear response behaviour of the Ge:Ga detectors (Tuffs & Gabriel, 2003).

Peschke & Schulz (2003) warned, however, that it is not obvious, that for a given observation the P32Tools provides the better photometric result. They found that for C200 P32 observations with low dynamic range data reduction using the standard PIA correction steps might be sufficient. For observations with high dynamic range (or with strong background fluctuations) reduction with P32Tools may provide better results. In the subsequent reduction we processed all observations in two different ways. The first scheme was the traditional PIA reduction without the P32Tools (see Table 1). The second option included the usage of P32Tools and the processing steps as described in Table 2. Before we compiled the final catalogue we compared the results of the two schemes (see Sect.5).

PIA data levels	Applied calibration and processing steps
ERD (Edited Raw Data) to	Ramp Linearization
SRD (Signal per Ramp Data)	Ramp Deglitching (2threshold method)
SRD to SCP	Reset Interval Correction
(Signal per Chopper Plateau Data)	Dark Current Subtraction (orbit dependent)
	Signal Linearization
	Signal Deglitching
	Combine signals
SCP to AAP	Calculate FCS responsivities
(Auto Analysis Product Data)	Flux calibration (convert signals to monochromatic flux densities per pixel)
at AAP level	**Drift correction**

Table 1: *Applied calibration and processing steps at different processing levels of PIA V10.0. Processing steps where separated IDL codes were used are typed in bold face.*

PIA data levels	Applied calibration and processing steps
ERD to SCP	Linearize ramps
	Dark current subtraction
	Reset Interval Correction
	Deglitching
	Transient Correction
SCP to AAP	Calculate FCS responsivities
(Auto Analysis Product Data)	Flux calibration (convert signals to monochromatic flux densities per pixel)
at AAP level	**Drift correction**

Table 2: *Applied calibration and processing steps at different processing levels of PIA V10.0, when P32Tools were used. Processing steps where separated IDL codes were used are typed in bold face.*

Flux calibration Since each observation is bracketed by two FCS measurements, there are several possibilities to combine the two responsivity values. We used the averaging method to calculate the responsivities during the flux calibration (it is the default method in PIA V10.0)

Drift correction A P32 measurement lasts typically several hundred seconds, and on this timescale slow baseline variations ('long term drift') could be significant. While for short-term transients P32Tools provides corrections, it does not offer solution for this issue. In order to correct for artifacts related to drift we performed a 2nd order polynomial fit to the data points per pixel. As a first step of this process we masked-out bright sources from the data stream, and a second order fit was applied to the remaining (background) points. Then the fitted curve was normalized by its average and each data point is divided by this resulting curve. This method worked well in those cases when the background level did not fluctuate significantly.

3.2 Flux extraction

In order to achieve good accuracies for photometry we used PSF fitting to extract fluxes from AAP data streams. The flux extraction process contains three subsequent steps: (1) AAP data points are resampled on the P32 "natural grid"; (2) point or extended nature of the object is checked; (3) the PSF of a point source or of a Gaussian shape extended source was fitted to the brightness distribution.

3.2.1 "Resampling on the P32 natural grid"

In a P32 observation the sky was sampled using the combination of the coarse raster steps of the spacecraft (in the Y and Z direction of the satellite coordinate system) and the sweeps of the focal plane chopper in the Y direction. Since the spacecraft pointing increment in the Y direction was constrained to be a multiple of the chopper step interval, these sampling resulted in a "natural grid" of P32 observations. Fig. 1 shows an example for the "natural grid" in the case of a C200 observation with raster dimension of 4×2 in Y×Z.

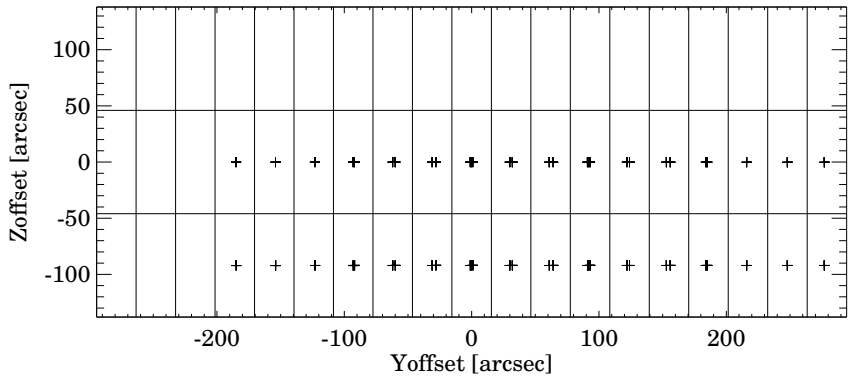

Figure 1: *P32 natural grid for the C200 observation of HR 6132. Pointing directions for 270 individual data points obtained with detector pixel #1 are denoted by crosses.*

We created maps on the natural grid by co-adding individual data points assigned to a specific grid point, per detector pixel. Thus four indepent pixel maps were generated, slightly shifted from each other. Outliers were removed taking into account the redundancy information (most map positions were observed several times).

3.2.2 Check for point/extended nature of the object

In order to choose the best PSF model during the flux extraction, we checked the point/extended nature of all detected sources. We fitted Gaussian profiles to the cross-scan values measured along the Y axis on individual pixel maps and extracted the FWHM value in each case (supposing that the specific pixel observed the source). The final FWHM was derived from the weighted average

of these values and the standard deviation σ_{FWHM} was also computed. Observations of Ceres at different wavelengths were used to define the Gaussian profile of a point source. An object was considered as extended source if its derived FWHM exceeded the FWHM of a point source by more than $3\,\sigma_{FWHM}$.

3.2.3 Extraction of fluxes from the maps

Each pixel provides a map about the studied region. Thus if a source is located close to the center of the raster the model fitting on the source could be performed on each map.

We used PSF fitting to extract fluxes from the maps. In the first step we estimated the positions of the detected brightness peaks in the map. Their coordinates were then compared with those of nearby SIMBAD sources. When likely candidate from SIMBAD could be identified (IRAS source, galaxy, etc.) then in the subsequent analysis we used the SIMBAD position rather than the ones estimated from the maps (due to the PSF sampling the accuracy of the estimated positions was usually not better than $10''$). In all other cases we used the measured ISOPHOT coordinates. If the specific source turned out to be point-like we used the measured beam profile (Ábrahám et al. 2007, in prep.) in the fitting. In spatially extended cases a Gaussian (with the FWHM measured above) model was used to calculate the footprint fractions at the map positions. Generally we assumed that the background was constant. In those cases when the sky brightness distribution showed a significant trend, we first performed a least-squares fitting of a plane to a set of marked background points, and then we subtracted the fitted plane from the data before the flux extraction.

In a usual P32 map with a source located at the centre of the raster, each detector pixel observed the target, producing four independent flux density values in the case of a C200 observation. Final source flux was derived from the average of these values, while uncertainty was computed as the standard deviation of the individual results.

4 Special cases

On some maps the detected source could not be identified unambiguously, since more than one SIMBAD objects were located close to the brightness peak (e.g. interacting galaxy pairs). In these cases we extracted photometry assuming a single source, but it is possible that several far-infrared sources contribute to the measured flux. In the catalogue we assigned the source most likely related to the measured parameters, but these observations are marked by a specific quality flag (see Appendix). Table 3 presents the affected sources, and lists the relevant TDT numbers.

There were several maps, which more than one well-separated brightness peaks could be detected on. In order to be compatible with the present structure of the ISO Data Archive, in these cases the catalogue and the assigned postcard and survey product only shows the basic parameters of the target closest to the centre of the map (usually this was the intended target of the observer). The data of additional sources, which are not included in the catalogue, are summarized in Table 4.

5 Comparison of the two data reduction method

As we described in Sect.3 we processed each observation using two different reduction schemes: (1) the standard PIA raster processing and (2) the P32Tools. In order to compare the efficiency of the two methods we collected those observations from the ISO Data Archive (IDA), where the target could be used as a standard object.

The photometric system of ISOPHOT is defined by a homogeneous set of 197 photospheric templates/models of 157 normal stars produced by M. Cohen and P. Hammersley. Of this

TDT number	Most probable source	Other source
16200714	NGC 3690	IC 694
16201115	APG 81	NGC 6622
19801212	NGC 5545	VV 210b
20501715	[SBM98] ACO 1691 J131102.02+391130.8	FIRST J131102.0+391131
26901254	UGC 9376	UGC 9376B
27700415	APG 81	NGC 6622
36202939	UGC 11628	KPG 548
36502321	APG 278	UGC 11985
37801072	KPG 579a	KPG 579b
37801168	KPG 572b	KPG 572
38302349	KPG 542a	KPG 542b
40500613	LEDA 51148	3C298
41801238	VV 296	MCG+02-38-020
42400415	VLSB F579-V01	VLSB F511-V01
42400856	VLSB F579-V01	VLSB F511-V01
61600227	NGC 4858	NGC 4860
71702942	NGC 5909	NGC 5912
75300912	NGC 6670	NGC 6670B
75301881	UGC 11453	MCG+09-32-008
77200490	UGC12480	MCG+01-59-030

Table 3: *List of observations where an additional source may contribute to the measured flux.*

TDT number	Original source	Additional source or sources	Wavelength [μm]	Flux density [Jy]	Flux uncertainty [Jy]
11400103	NGC 6045	IC 1179	170	0.89	0.05
11400107	IC 1191	IC1189	170	0.90	0.06
65400820	[JCC87] IRAS 4A	IRAS 03259+3105	200	550	33.0
	[JCC87] IRAS 4A	IRAS 03259+3105	200	509	77.0

Table 4: *Photometry of additional sources which were observed in maps centred on the main targets of the observers ("original source").*

collection 24 stars were actually used at $\lambda \leq 25\mu$m and 12 at longer wavelengths. In order to extend the calibration to higher fluxes asteroids (Müller & Lagerros 2002) and planets (Griffin & Orton) were involved as well.

During the ISO mission only a low number of standard objects were observed in the P32 mode with the C200 detectors. Our search in the IDA resulted in 14 standard observations (7 observations for stars, 5 for Ceres, 2 for Uranus). In terms of predicted flux densities these objects cover the low flux level (<0.5 Jy, stars) and the very high flux level (>40 Jy, Ceres, Uranus) only.

In Fig. 2 we plotted the ratio of the colour corrected measured fluxes to the predicted fluxes as the function of predicted fluxes for these standard objects. At low flux levels the simple PIA reduction provides slightly better results, while in the case of very bright sources (>30 Jy) the maps produced by P32Tools seems to be more reliable. However, the "predicted flux" (x-axis) is not known for most sources. A more practical approach is shown in Fig. 3 where on the x-axis we plotted the dynamic range of the maps. The dynamic range is defined as the difference between peak signal and average background signal within the map, measured in V/s on the PIA based images. Since the dynamic range is a measurable quantity Fig. 3 can be directly used to select the most suitable data reduction method. The conclusions from this figure agree well with those from Fig. 2: while for faint sources the PIA based maps turned out to be slightly more reliable, for bright sources the usage of P32Tools is recommended. As a consequence, for observations of dynamic range less than 0.05 V/s we used results extracted from maps reduced by the standard PIA routines. For observations of higher dynamic ranges (>0.05 V/s), maps produced by the P32Tools were used. There were, however a few cases, when we deviated from this scheme, and used the P32Tools also for maps of low dynamic range, for the sake of better deglitching or drift

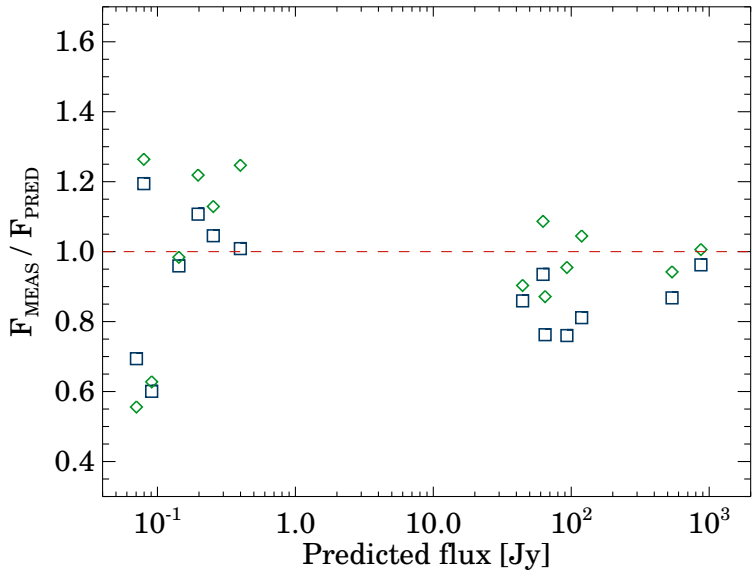

Figure 2: *Ratio of the measured flux densities to the predicted flux densities against predicted flux densities for the selected standard objects. Blue squares mark the results of the simple PIA reduction, green diamonds show the corresponding ratios obtained by the usage of P32Tools.*

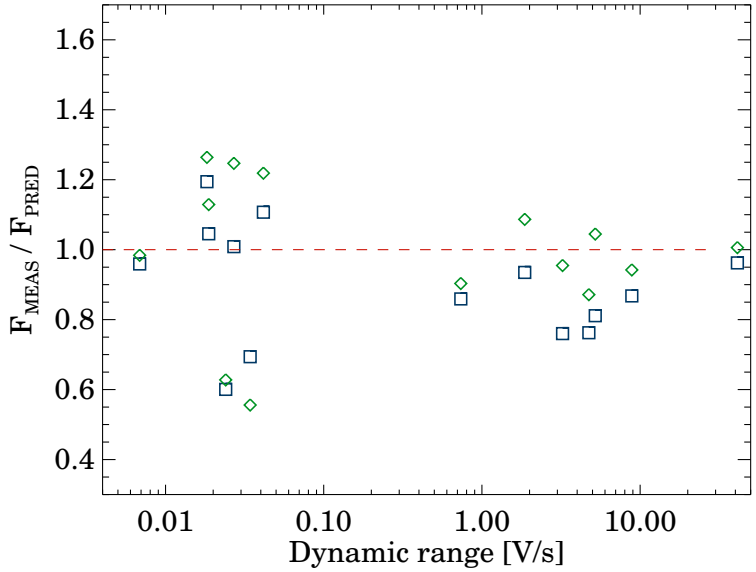

Figure 3: *Ratio of the measured flux densities to the predicted flux densities against the dynamic ranges measured on maps reduced by the PIA.*

correction.

In order to extend further our database of objects with independent flux estimates, we searched the Archive for objects, which (1) were measured both in the PHT32 mode and in the PHT22 raster mode at the same wavelength; (2) presumably do not show strong variability in the far-infrared or measured at the same epoch in both modes (e.g. IRAS17208-0014 which was measured in the framework of the PHT_CAL programme at revolution 843 in the PHT32 and PHT22 mode as well); (3) are presumably compact sources. This search resulted in seven

additional observations. The publicly available ISO Data Archive contains the relevant flux densities (and their uncertainties) for most of these PHT22 observations as Highly Processed Data Products (Moór et al., 2005, 2006). To extract the flux from the P22 observation of IRAS17208-0014 (which is not included in these catalogues) we used the same scheme as described by Moór et al. (2003).

In Figure 4 we plotted the ratio of the measured flux densities to the expected flux densities (predicted fluxes for the standard objects, and measured fluxes for other objects) against expected flux densities. Taking into account these additional standards the uncertainty numbers are not changed: the 1σ uncertainty is $\sim$45 mJy below 0.5 Jy, and $\sim$10% for brighter sources. This is comparable to the accuracy of observations obtained in mini-map mode.

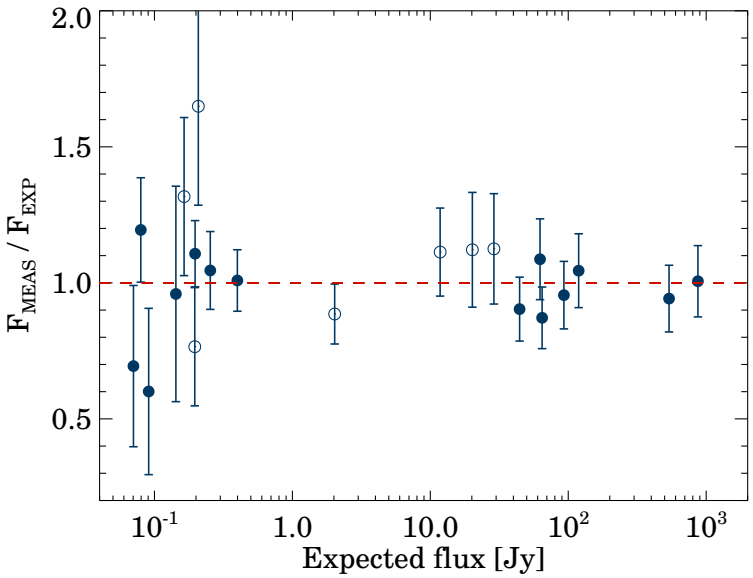

Figure 4: *Ratio of the measured flux densities to the expected flux densities against expected flux densities for the selected standard objects (filled circles) and for the seven additional objects (circles).*

Acknowledgment

We thank Dr. Richard Tuffs for the one week long training course held in the topic of data reduction of P32 observations.

References

Acosta-Pulido, J. A., Gabriel, C., & Castañeda, H. 2000, Experimental Astronomy 10, Kluwer Academic Publishers, 333-346

Gabriel C., Acosta-Pulido, J., Heinrichsen, I., et al., 1997, in Proc. of the ADASS VI conference (Eds.: G. Hunt, H.E. Payne, ASP Conf.Ser. 125), 108

Moór, A., Ábrahám, P., Kiss, Cs., Csizmadia, Sz., 2003, "Far-infrared observations of normal stars measured" with ISOPHOT in mini-map mode (http://pma.iso.vilspa.esa.es:8080/hpdp/technical_reports/technote5.pdf)

Moór, A., Ábrahám, P., Kiss, Cs., Csizmadia, Sz., 2005, "Far-infrared ISOPHOT minimaps of extragalactic objects" (http://pma.iso.vilspa.esa.es:8080/hpdp/technical_reports/technote30.html)

Moór, A., Ábrahám, P., Kóspál, Á., Juhász, A., Kiss, Cs., 2006, "ISOPHOT Catalogue of Young Stellar Objects" (http://pma.iso.vilspa.esa.es:8080/hpdp/technical_reports/technote46.html)

Müller, T. G., & Lagerros, J. S. V. 2002, A&A, 381, 324

Peschke, S. B., & Schulz, B. 2002, ESA SP-482: Photometric Mapping with ISOPHOT using the "P32" Astronomical Observation Template, 53

Tuffs, R. J., & Gabriel, C. 2003, A&A, 410, 1075

Tuffs, R. J. et al., 2006, Far-Infrared ISOPHOT Photometry of late-type Virgo Cluster Galaxies (http://pma.iso.vilspa.esa.es:8080/hpdp/technical_reports/technote45.html)

Appendix: description of the catalogue

The flux densities and their uncertainties resulted from the data reduction described in this document, were listed in a photometric catalogue which is included as Highly Processed Data Product. In the following we shall describe the fields of the catalogue.

Column	Field	Unit	Description
(1)	Object name		SIMBAD compatible name or target name as given by the original ISO proposer.
(2)	Object type		Standard SIMBAD code for object type.
(3)	ISO name		Object name given by the ISO observer.
(4)	TDTNUM_ON		The 8-digit TDTNUM of the on-source observation.
(5)	On_ Meas.		Index of the on-source measurement within TDTNUM_ ON.
(6)	RA(2000)		Right ascension, h:m:s.
(7)	Dec(2000)		Declination, d:m:s.
(8)	Detector		ISOPHOT detector (C200).
(9)	Wavelength	[micron]	Nominal wavelength of the ISOPHOT filter.
(10)	Aperture	[arcsec]	Aperture for detectors square for the C200 detector.
(11)	Epoch		Epoch of the observation.
(12)	TDTNUM_ OFF		The 8-digit TDTNUM of the off-source observation.
(13)	Off_Meas.		Index of the off-source measurement within TDTNUM_OFF.
(14)	Flux density	[Jy]	Flux density of the source. In case of a point source the measured flux is corrected for the size of the point spread function. In case of an extended source it corresponds to the integrated brightness. No colour correction applied.
(15)	Flux uncertainty	[Jy]	Flux uncertainty. No colour correction applied.
(16)	Background	[MJy/sr]	Background surface brightness. No colour correction applied.
(17)	Object size		Indicates if the object is point-like (P) or extended (E).
(18)	Quality		Quality of the observation. R1 – Standard processing according to the scheme described in the report. R2 – Observation was carried out at the very beginning or at the very end of orbit. Reduced photometric reliability at orbital phase lesser than 0.2. R3 – The detected source could not be identified unambiguously, because more than one SIMBAD objects were located close to the brightness peak. It is possible that several far-infrared sources contribute to the measured flux. R4 – ISOPHOT position differs from SIMBAD position by more than $20''$.

Table 5: Description of the catalogue